THE B/C AND SUB-IRON/IRON COSMIC RAY RATIOS - FURTHER EVIDENCE IN FAVOR OF THE SPIRAL ARM DIFFUSION MODEL

David Benyamin[1], Ehud Nakar[2], Tsvi Piran[1] & Nir J. Shaviv[1,3]

1. The Racah Institute of physics, The Hebrew University of Jerusalem, Jerusalem 91904, Israel
2. Raymond and Beverly Sackler School of Physics & Astronomy, Tel Aviv University, Tel Aviv 69978, Israel and
3. School of Natural Sciences, Institute for Advanced Study, Einstein Drive, Princeton, NJ 08540

ABSTRACT

The Boron to Carbon (B/C) and sub-Fe/Fe ratios provides an important clue on Cosmic Ray (CR) propagation within the Galaxy. These ratios estimate the grammage that the CR traverse as they propagate from their sources to Earth. Attempts to explain these ratios within the standard CR propagation models require ad hoc modifications and even with those these models necessitate inconsistent grammages to explain both ratios. As an alternative, physically motivated model, we have proposed that CR originate preferably within the galactic spiral arms. CR propagation from dynamic spiral arms has important imprints on various secondary to primary ratios, such as the B/C ratio and the positron fraction. We use our spiral arm diffusion model with the spallation network extended up to Nickel to calculate the sub-Fe/Fe ratio. We show that without any additional parameters the spiral arm model consistently explains both ratios with the same grammage, providing further evidence in favor of this model.

Subject headings: cosmic rays — diffusion — Galaxy: kinematics and dynamics

1. INTRODUCTION

Cosmic ray (CR) composition measurements have been collected for almost four decades. Their analysis provides information on the propagation through the interstellar medium (ISM), which further provides information on the CR sources and various properties of the ISM. One of the most important aspects characterizing the propagation is the CR path length distribution (PLD), which describes the probability distribution function of the path lengths traversed by CRs between their origin and their measurement near Earth. This PLD determines the amount of spallation and radioactive decay the particles will undergo on the way to Earth. Thus, by measuring the ratio between secondary CR particles, formed en route, to primary particles accelerated at the source, one can constrain the PLD.

Until recently one of the stringent and often implicit assumptions in CR propagation models was an azimuthally symmetric source distribution (e.g. Strong et al. 2007; di Bernardo et al. 2010). The PLD resulting from such models closely resembles an exponential PLD.

One of the problems in these disk-like models is the amount of grammage the models require to explain the B/C and the sub-Fe/Fe ratios given the same geometric parameters. Because of the higher spallation cross-sections, the sub-Fe/Fe ratio is typically sensitive to the relative fraction of short path lengths in the PLD. The B/C ratio, with lower spallations cross sections, is more sensitive to the relative fraction of long path lengths. When trying to fit both measured ratios simultaneously in a disk-like model, one finds inconsistency with the nearly exponential PLD of the disk-like models—the sub-Fe/Fe ratio requires a larger mean grammage than the B/C ratio. Garcia-Munoz et al. (1987) suggested that this inconsistency could be resolved with the ad hoc assumption that short path lengths are suppressed.

In a different analysis, Davis et al. (2000) investigated whether the introduction of a second, low-energy CR source can reproduce the B/C and sub-Fe/Fe ratios, in particular, at low energies. Although they found that one can recover the B/C ratio and the sub-Fe/Fe ratio separately, they were unable

to find any combination of parameters that fit both ratios simultaneously, for the aforementioned reason. Namely, Iron nuclei do not produce enough secondaries given model parameters that correctly reproduce the B/C.

Over the past decade, CRs propagation models evolved to include spiral arms as the source of the CR particles (Shaviv 2003; Shaviv et al. 2009; Gaggero et al. 2013; Effenberger et al. 2012; Werner et al. 2013). In these models, the CR sources primarily reside at a finite distance from the solar system, and this naturally suppresses the short path lengths (e.g., see figs. 4 and 6 in Benyamin et al. 2014, hereafter B14). Hence, spiral arm models could in principle fit both ratios with the same model parameters. We study this possibility here.

B14 considered the spiral arms to be dynamic as well, showing that this model recovers the low energy behavior of the B/C ratio. More specifically, secondaries to primaries ratios such as the B/C, are expected to decrease with energy because the time required for particles to reach the solar system (i.e., their "age") decreases with the diffusivity, which increases with the energy. However, below 1 GeV/nuc., the B/C ratio exhibits the opposite behavior. Although unexpected from just diffusion, it can be explained by taking into account the dynamics of the spiral arms. This is because at sufficiently low energies the CR age will be governed not by the diffusion from the spiral arms but instead by the time since the last spiral arm passage, which would be shorter. Since CRs below 1 GeV/nuc. are non-relativistic, an energy independent propagation time then gives less spallation products at lower energies, thus reproducing the B/C rise at low energies (B14), without requiring any additional assumptions on the propagations (such as a galactic wind, reaccaleration or breaks in the diffusion coefficient).

One interesting ramification of the modified PLD of the spiral arm model is that it requires a notably smaller halo size and diffusion coefficients to recover the observed B/C and ^{10}Be/Be ratio. Namely, by modifying the PLD one has to change the "canonical" diffusion parameters characterizing the cosmic rays (B14). This is reasonable and even expected

given that those "canonical" parameters were obtained within the standard disk-like model whose propagation characteristics are quite different from those of the spiral arm model that we consider here.

An interesting related phenomenon is the unexpected energy dependence of the positron fraction, $e^+/(e^+ + e^-)$, of CRs. Since positrons in standard scenarios are secondary particles, the ratio is expected to decrease with energy (Moskalenko & Strong 1998). However, the PAMELA satellite measurements revealed that the ratio increases with the energy above 10 GeV up to at least 100 GeV (Adriani 2009). More recent measurements by AMS-02 show leveling at 300 GeV (Accardo et al. 2014).

Given that standard models could not explain this behavior, several solutions were suggested. The increased positron fraction at higher energies can be explained in any scenario having an additional primary population of pairs with a hard spectrum, such that it dominates the population of secondary positrons above 10 GeV. Pairs can naturally be created by dark matter annihilation (Bergström et al. 2008; Ibarra & Tran 2008), by pulsars (Harding & Ramaty 1987, Chi et al. 1996, Aharonian et al. 1995, Hooper et al. 2009, and Profumo 2008) or in aged SNRs (Blasi 2009, Blasi & Serpico 2009, Ahlers et al. 2009, and Mertsch & Sarkar 2009).

Another type of explanation directly related to the PLD was proposed by Shaviv et al. (2009). If the CR sources are concentrated at a finite distance from the solar system, as is expected from the spiral arm structure, the paucity of short path lengths implies that primary electrons with a high enough energy will cool before reaching the solar system. In contrast, the secondary positrons are formed by protons that effectively do not cool, such that they can be formed in the solar system's vicinity. For the local electron cooling rate determined by Synchrotron and inverse-Compton scattering, and the typical CR age determined by Beryllium isotope ratios, this behavior predicts that the Positron fraction should start increasing above 10 GeV, thus explaining the "Pamela Anomaly", effectively without any free parameters.

In the present work we study the B/C and sub-Fe/Fe ratios using an extended version of the B14 model, as is described in §2.1. One of the major uncertainties arising when studying the sub-Iron to Iron ratio and its implications to the PLD, is the energy dependent spallation cross-sections. Since many of the partial cross-sections are poorly measured, the values used are often the results of fits and extrapolations, giving rise to large uncertainties (Moskalenko 2011; Webber et al. 2003). The problem is aggravated below a few GeV/nuc., where the cross-sections have larger energy dependences (Moskalenko & Mashnik 2003; Schwaller et al. 1979), and for heavier elements (e.g., see appendix II in Garcia-Munoz et al. 1987; Titarenko et al. 2008; Sisterson & Vincent 2006). We limit the analysis to energies between 10 GeV/nuc. to 1000 GeV/nuc. Although it is not clear by how much it decreases the uncertainties in the cross-sections, the weaker energy dependence will translate into a smaller uncertainty in the inferred spectral slope of the diffusion coefficient. We use the nominal model parameters of B14, as summarized in §2.3, and search the optimal diffusion coefficient spectral index and normalization, namely, δ, and D_0 in $D = D_0(E/E_0)^\delta$ [1], with $E_0 = 3$ GeV/nuc., to fit both the B/C from AMS-02 (Oliva et al. 2013) and the sub-Fe/Fe data from HEAO-3 (Binns et al.

1988) and SANRIKU (Hareyama 1999). We carry out the analysis twice, once for a disk-like model having no spiral arms, and once for the spiral arm model of B14.

We begin in §2 by briefly describing the model we developed in B14 and the parameters we use. In §2.1 we detail the improvements carried out for the present work. The results are then described §4, the main part of which includes separate fits of δ, and D_0 to the observed B/C ratio and to the sub-Fe/Fe ratio. The implications of these results are then discussed in §5.

2. THE NUMERICAL MODEL

In B14 we developed a CR advection-diffusion model with which we recovered the B/C ratio. The nuclear network in the model included all stable and long lived radioactive isotopes between Beryllium and Oxygen. The model followed the propagation of primary and secondary CRs from their sources, primarily located on spiral arms. Unlike present day state of the art simulations (such as GALPROP, Strong et al. 2007 and DRAGON, di Bernardo et al. 2010) that solve the partial differential equations of the describing advection and diffusion, our model uses a Monte Carlo (MC) algorithm.

Instead of simulating the small steps corresponding to the physical mean free path (m.f.p.) of the CRs, around 1 pc, our MC simulation uses a larger effective m.f.p., which lumps together many small effective physical steps. This corresponds to a larger effective time step chosen to be $\tau_{esc}/100$, where $\tau_{esc} \approx Z_h^2/2D$ is the typical escape time of a CR from the galaxy[2]. In the present simulations, we fix Z_h to be 250 pc, like our nominal model in B14. This corresponds to an effective m.f.p. of 25 pc, Which is smaller than the typical length scale over which the gas density varies.

Each time step, we check whether the CR bundle had left the galaxy. If it did not, we calculate the grammage that the bundle traversed in this time step. We then calculate the probability that the particles had undergone a nuclear reaction with ISM. If the particles did undergo spallation into secondary particles, we follow the latter with the same methodology. We nominally use the YIELDX subroutine of Silberberg & Tsao (1990) for the nuclear cross-secitons. However, we repeat the analysis with Webber et al. (2003) to obtain a handle on the uncertainty introduced by the nuclear cross-sections, as described below. For long-lived radioactive isotopes, we also check each time step for radioactive decay. The code also considers Coulomb and ionization losses as elaborated in Mannheim & Schlickeiser (1994) and applied in GALPROP (Strong & Moskalenko 1998).

For the present simulations, each run uses 10^9 CR bundles in the spiral arms simulations and 10^8 in the disk-like simulations. For each bundle, we randomly choose its initial isotopic identity and initial location in the galaxy, and follow it until it escapes the galaxy, cool below the 10 GeV/nuc., break into isotopes lighter than the lightest element simulated or reach the solar vicinity. In the latter case we record all simulated isotopes (Beryllium to Silicon in the light elements simulations and Scandium to Nickel in the heavy elements simulations), in a 3D array (Z, A, energy). The energies are recorded in 10 bins per decade, covering the range of 10 GeV/nuc. to 1000 GeV/nuc..

2.1. *The extended code*

---

[1] Throughout the paper, the term "diffusion coefficient" actually refers to the normalization D_0 and not $D(E)$.

[2] Although the time step $\delta t(E)$ is energy dependent, the effective m.f.p. is not, as it depends on the combination $\delta t(E) \times D(E)$.

Below we detail specific modifications and improvements of the code used in this work.

2.1.1. *Nuclear network*

As we are interested in second order corrections to the B/C ratio, we extended the code to describe the spallation network all the way up to Silicon.

In addition to the range of "light" elements necessary for the aforementioned calculation, we are also interested in calculating the sub-Fe/Fe ratio. We therefore added the nuclear network of heavier elements, from Scandium to Nickel as well, using the YIELDX (Silberberg & Tsao 1990), or alternatively Webber et al. (2003) for the partial spallation cross-sections describing the interaction with Hydrogen. We use the approximate formulae of Karol (1975) for the total inelastic cross-sections of interactions with Helium.

2.1.2. *Faster code*

The code was accelerated by limiting the CR diffusion in the spiral-arms models to take place only within of a radius 5 times the halo size around the solar system. This captures 97% of the total CRs reaching the solar system, when comparing to a full calculation without the distance cutoff, but increases the speed by about an order of magnitude to reach similar statistics. For the disk-like model simulations, this is unnecessary. The azimuthal symmetry allows for much better statistics than the spiral-arms simulation with much fewer CR bundles.

In order to increase the accuracy, we decrease the time step 10-fold when the CR bundle is within a distance of 150 pc from the solar system, an additional 10-fold when the bundle is within 120 pc, and we take a time step for which the effective mean free path (m.f.p.) is of order the actual physical m.f.p. (of order 1 pc), when the CR bundle is within 100 pc from the solar system.

2.2. *Initial composition*

The initial composition for which we obtain the optimal fit to the measured secondary/primary isotope ratios in the light elements simulations is 37% Carbon (by number), 3% Nitrogen, 52% Oxygen, 4% Neon, 2% Magnesium and 2% Silicon. Note that although the method for finding the initial composition is the same as in B14, the composition is somewhat different because the code now follows more isotopes, as described in §2.1.1. For the heavy elements simulations, the best fit to the observed Ni/Fe ratio, is obtained for an initial composition consisting of 95% Iron and 5% Nickel.

2.3. *The nominal model parameters*

Table. 1 summarizes the nominal model parameters obtained by or referenced within B14. These parameters are separately fixed for either the spiral-arms simulations or the disk-like simulations.

3. OBSERVATIONAL DATASETS

We compare the model predictions for the B/C ratio with the AMS-02 results, whose advantage over previous datasets is the notably better statistics. In total, there are 10 data points between 10 GeV/nuc. and 1000 GeV/nuc. (Oliva et al. 2013).

The sub-Fe/Fe datasets used both the HEAO-3 (Binns et al. 1988) and the SANRIKU measurements (Hareyama 1999). In total, there are 21 data points between 10 GeV/nuc. and 1000 GeV/nucleon.

TABLE 1
NOMINAL MODEL PARAMETERS

parameter	definition	value for spiral arm model	value for disk-like model
Z_{h}	Half halo height	250 pc	1kpc
τ_{arm}	Last spiral arm passage	5 Myr	
i_4	4-arms set's pitch angle	28°	
i_2	2-arms set's pitch angle	11°	
Ω_4	Angular velocity of the 4-arms set	15 (km/s) kpc^{-1}	
Ω_2	Angular velocity of the 2-arms set	25 (km/s) kpc^{-1}	
$f_{\mathrm{SN},4}$	Percentage of SN in the 4-arms set	48.4%	
$f_{\mathrm{SN},2}$	Percentage of SN in the 2-arms set	24.2%	
$f_{\mathrm{SN,CC}}$	Percentage of core collapse SNe in the disk	8.1%	80.7%
$f_{\mathrm{SN,Ia}}$	Percentage of SN Type Ia	19.3%	19.3%

4. RESULTS

We have separately fitted the B/C data and the sub-Fe/Fe data to the two CR source models: the spiral arms sources, and a disk-like, azimuthally symmetric, one. For each model we then checked its consistency, as the different datasets (B/C and sub-Fe/Fe) should be fitted with the same models parameters. If we find consistency the optimal parameters then teach us about CR diffusion in the interstellar medium.

To obtain the best fit values, we minimize the χ^2 for each simulation. The uncertainty used in estimating the χ^2 values include both those arising from the (Monte Carlo) simulation and the quoted observational errors which are typically an order of magnitude larger.

4.1. *B/C*

The fit to the optimal spectral slope δ and diffusion coefficient D_0 is carried by calculating the χ^2 over a two dimensional array of values. Then, the set of χ^2 for each value of δ in the range of 0.3 to 0.7 is fitted with a polynomial, and the minimum found.

The optimal diffusion coefficient as a function of δ is given in table 2. By comparing the disk-like models to the spiral arm models, it is evident that the typical D_0 required to fit the observations in "standard" disk-like models is much larger than the typical D_0 required to fit the same data in the spiral arm model. This recaptures the result previously described in B14, and arises from the smaller halo in the spiral arm model.

The model fits to the data, as a function of δ, are depicted in fig. 1 for the disk-like model and fig. 2 for the spiral arm model. One sees from these fits that one requires roughly the same $\delta \sim 0.4$ (thicker purple line) to fit both the disk-like and spiral arm models.

Figs. 5 & 6 depict the χ^2 as a function of both δ and D_0.

The latter plots also demonstrate that for a given value of δ there is a narrow range of D_0 for which there is a reasonable fit. However, without prior knowledge of δ, there is a much wider allowed range for optimal D_0.

4.2. *Iron*

Independently of fitting the B/C data, we fit the sub-Iron to Iron data in a similar way. The model fits to the Iron data as a function of δ, are depicted in fig. 3 for the disk-like model
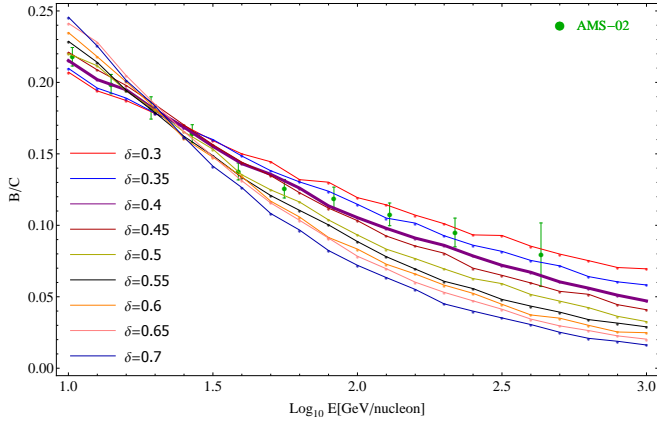
FIG. 1.— The optimal χ^2 fit of the B/C data for several δ values in the range 0.3 to 0.7, for disk-like simulations. Data is taken from Oliva et al. (2013). The thicker purple line corresponds to the overall best fit, with $\bar{\delta} = 0.45$.
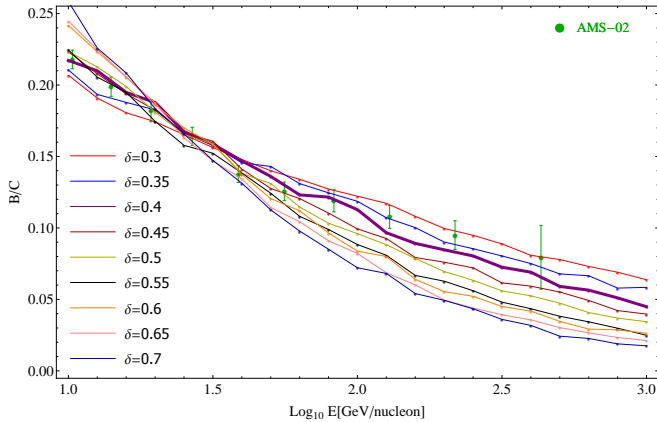

FIG. 2.— Similar to fig. 1 but for the spiral arm model. The overall optimal fit here is also $\delta = 0.45$.

FIG. 3.— The optimal χ^2 fit of the sub-Fe/Fe data for a set of δ's between 0.3 to 0.7, in disk-like simulations. The thicker mustard colored line corresponds to the overall best fit, with $\delta = 0.5$. Data taken from HEAO-3 (Binns et al. 1988) and SANRIKU (Hareyama 1999).

FIG. 4.— Similar to fig. 3 but for the spiral arm model. Unlike the disk-like model, the overall optimal fit here is $\delta = 0.35$ depicted a thick blue line.

and fig. 4 for the spiral arm model. Unlike the B/C fits, here the optimal fits require a different δ values for the two models. For the disk-like model, the optimal is $\delta \sim 0.5$ while it is $\delta \sim 0.35$ for the spiral arm model. The source of the difference points to an interesting physical effect associated with the different path length distribution. Because the cross-section of the heavier elements is larger, their mean free paths are much smaller relative to the distance traversed, thus giving rise to saturation (especially at lower energies), whereby an increase in the grammage does not increase as much the ratio between secondary and primary isotopes. This saturation causes a decreases in the secondary/primary slope. However, because of the different path length distribution, the effect is notably larger for the disk like model with an exponential PLD. Thus, in order to compensate for this effect, one requires a steeper diffusion power law index to explain the small observed slope. For the spiral arm model, the saturation is less important such that the diffusion power law index should be closer to the observed sub-Fe/Fe slope.

Figs. 5 & 6 show the χ^2 as a function of both δ and D_0.

4.3. *B/C vs. sub-Fe/Fe comparison*

The above analysis was carried out separately with B/C and sub-Fe/Fe data sets. However, any consistent model should be able to fit both datasets with the same model parameters. This implies that the χ^2 contours depicted in figs. 5 & 6 should overlay each other. A quick inspection reveals that only the spiral arm model gives consistent parameters, with
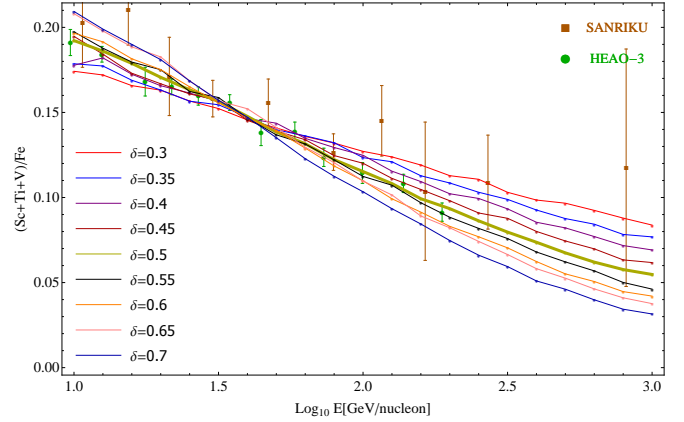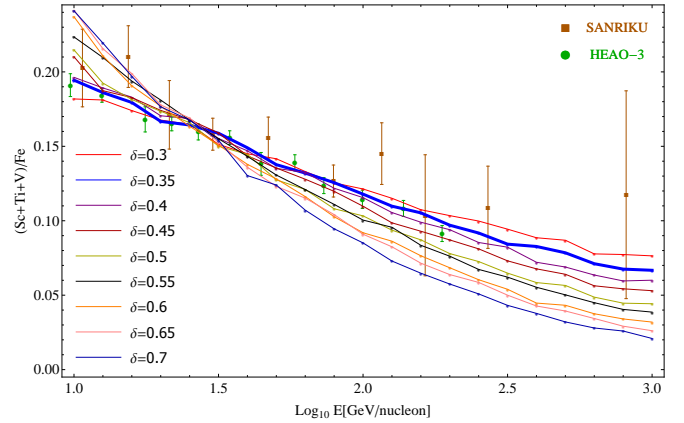
$D_0 \sim 10^{27} \mathrm{cm^2 s^{-1}}$ to $1.2 \times 10^{27} \mathrm{cm^2 s^{-1}}$ and $\delta \sim 0.35-0.45$. This can also be seen in table 2. While the disk-like model requires a similar δ to fit both datasets, the iron data requires a diffusion coefficient that is of order 35% smaller from the diffusion coefficient required to recover the B/C data, for any given δ. The smaller diffusion coefficient corresponds to a larger grammage. This recaptures the claims raised by Garcia-Munoz et al. (1987), that the sub-Fe/Fe data requires a larger grammage than the B/C data requires. Here we limit ourselves to high energies (>10 GeV/nuc.) where we expect smaller uncertainties in the energy dependence of the cross-sections, and reach the same conclusion.

This inconsistency is manifested in the minimum $\chi^2/\mathrm{d.o.f.}$ (per degree of freedom) obtained in the combined analysis. For the disk-like model, we find $\chi^2/\mathrm{d.o.f.} = 3.66$ with $\mathrm{d.o.f.} = 31 - 2 = 29$. However, for the spiral arm model it is $\chi^2/\mathrm{d.o.f.} = 0.95$, for the same number of degrees of freedom. Formally, this implies that the disk like model can be ruled out at the 10^{-10} level.

To see how sensitive this conclusion is to the nuclear cross-sections employed, we repeated the analysis with the cross-sections of Silberberg & Tsao (1990) replaced with those of Webber et al. (2003). The results are depicted as the dashed contours in figs. 5 and 6. Evidently, the discrepancy remains though it is more than twice smaller. In other words, the uncertainties in the cross-sections are sufficiently large that one cannot unequivocally use the B/C and sub-Fe/Fe data to

rule out a disk-like model, though it is inconsistent with the present spallation cross-sections.

One should emphasize that the actual values of the diffusion coefficients are less certain than from these fits. This is because we set the nominal halo sizes for the two models. Changing the halo sizes would also scale the values of the optimal D_0 obtained. While this introduces an uncertainty in the actual values of D_0 this will not resolve the inconsistency between the two data sets in the disk-like models and will not introduce any inconsistency for the spiral arm model. That is, the scaling would be the same for both the B/C and sub-Fe/Fe such that the consistency (in the spiral arm model) or inconsistency (in the disk-like model) between the dataset fits would remain.
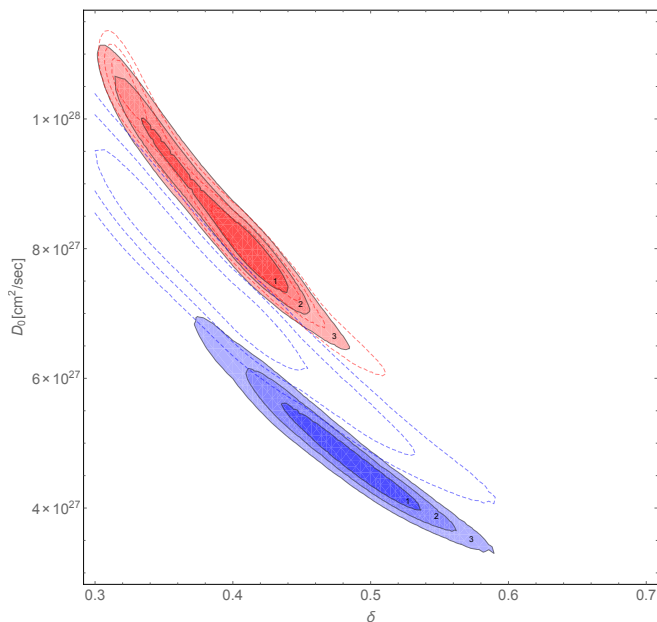

FIG. 5.— A contour plot of χ^2 for the disk-like model. The red contours correspond to the B/C fit. The blue contours correspond to the sub-Fe/Fe fit. The dashed lines correspond to the same contours as obtained when replacing the cross-sections of Silberberg & Tsao (1990) with those compiled by Webber et al. (2003). Note that the discrepancy between the B/C and the sub-Fe/Fe derived model parameters decreases, but still remains.

TABLE 2
THE OPTIMAL D_0 IN UNITS OF 10^{27}CM^{2}S^{-1} AS OBTAINED FOR THE TWO MODELS, WHEN SEPARATELY FITTING THE B/C AND THE SUB-FE/FE DATA.

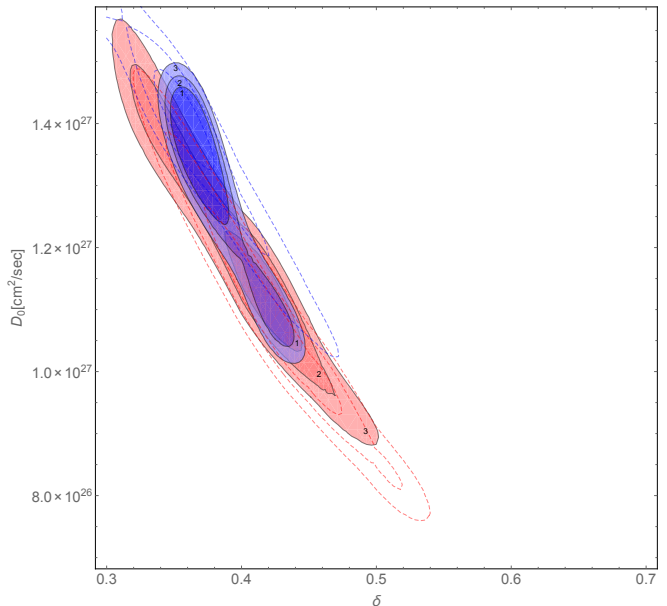|	D_0 from spiral arm model		D_0 from disk-like model	
δ	B/C	sub-Fe/Fe	B/C	sub-Fe/Fe
0.3	1.6	1.65	10.9	8.8
0.35	1.37	1.4	9.5	7.4
0.4	1.17	1.2	8.2	6.2
0.45	1.03	1.01	7	5.3
0.5	0.89	0.9	6.2	4.5
0.55	0.8	0.74	5.5	3.8
0.6	0.65	0.66	4.7	3.2
0.65	0.58	0.56	4	2.6
0.7	0.5	0.5	3.6	2.3

FIG. 6.— A contour plot of χ^2 for the spiral arm model. The red contours correspond to the B/C fit. The blue contours correspond to the sub-Fe/Fe fit . The dashed contours are similar to those in fig. 5.

5. DISCUSSION & SUMMARY

In previous work, we developed a fully 3D CR diffusion model which not only considers that most CR acceleration takes place in the vicinity of spiral arms, but also that these arms are dynamic (Benyamin et al. 2014). It was shown that by adding these observationally based components to the model, one recovers observed secondary to primary ratios, such as of Boron to Carbon. In particular, it was found that the ratio increases with energy below 1 GeV/nuc. and decreases above this energy, instead of the monotonic decrease with energy expected in the simplest galactic diffusion model (e.g., Cesarsky 1980, without having to assume additional assumptions, such as reacceleration or a galactic wind). This is because the age of the CRs at low energies is not determined by the diffusion time from the spiral arms, but instead governed by the (energy independent) time since the last spiral arm passage. Since below 1 GeV/nuc., the particles are non-relativistic, a fixed age translates into a grammage which is increasing with energy, and correspondingly an increasing secondary to primary ratio at low energies.

One very important aspect of this model is that the path length distribution is different from the one found in standard diffusion models. In the latter, the PLD is typically close to being exponential. However, if most CRs arrive from a distance, then the PLD will show a paucity of small path lengths (compare fig. 4 to fig.6 in B14).

The different PLD has an interesting ramification. CRs arriving after having passed a short path length necessarily remain close to the galactic plane. In contrast, CRs having a long path length could stray further from the plane before returning back. Since the ISM density falls with the distance from the plane, CRs with short paths therefore experience a higher average ISM density than CRs with long paths. Thus, a distribution which is missing the short path lengths, as is the case in the spiral arm model, will have a lower average interaction with the ISM for a given average path length. In other words, the average grammage will be lower for the same average physical length. This result implies that if the spiral

Benyamin et al.

arm model is to recover the observed secondary to primary ratio, the model has to keep the CRs closer to the galactic plane where the density is higher. For this reason, the typical halo size required to fit the same secondary to primary ratio data is lower (typically a few hundred pc, compared with the 1 to 4 kpc in more standard diffusion models). However, because the typical age is closely related to the ratio between the radioactive and stable Beryllium isotopes, which is a model independent observation, the smaller halo requires a smaller diffusion coefficient. At 1 GeV/nuc. it should be of order 10^{27} and not $10^{28} \mathrm{cm}^2 \mathrm{s}^{-1}$.

Here we extended the model developed in B14, as detailed in §2.1. In particular, we enlarged the spallation network to describe the spallation of Iron and Nickel as well as their spallation products. Thus, we could predict the sub-Fe/Fe ratio as a function of model parameters, in addition to the B/C ratio. We carried a parameter study whereby we fit both the spectral slope δ of the diffusion coefficient and its normalization D_0 (while keeping the other model parameters fixed at their nominal values). This was carried out twice, for a ("standard") disk-like model and for a spiral arm model, in the energy range of 10 GeV/nuc. - 1000 GeV/nuc.. The reason for focusing on high energies is to avoid the notorious uncertainties associated with the spallation cross-sections at lower energies (e.g., Moskalenko 2011; Webber et al. 2003). These uncertainties become more acute as Z increases (see Titarenko et al. 2008; Sisterson & Vincent 2006 and also Appendix II in Garcia-Munoz et al. 1987).

In a standard disk-like model, we find an inconsistency between the diffusion coefficient required to fit the B/C and the value required to fit the sub-Fe/Fe ratio. Phrased differently, it implies that the sub-Fe/Fe ratio requires more grammage than the B/C ratio. One way to resolve the inconsistency present in the standard disk-like model would be to modify the cross-sections at the higher energies over which the fit to observational data was carried out. This is not inconceivable given that by replacing the cross-sections of Silberberg & Tsao (1990) with those of Webber et al. (2003), we reduce the discrepancy by more than a factor of 2.

Another way to resolve the inconsistency within the standard disk like model would be to truncate the short paths lengths by letting the CRs interact with material at the SNR. This explanation which was originally proposed to resolve the PAMELA anomaly (**?**), would requires however additional free parameters. A priori it is not clear that the parameters that resolve the PAMELA anomaly would also resolve this inconsistency.

A spiral arm source distribution consistently requires the same diffusion coefficient (or grammage) when fitting the sub-Fe/Fe and B/C datasets. This arises because the average mean free path for spallation of Iron is notably smaller than that of Carbon and Oxygen, such that the sub-Fe/Fe and the B/C are not sensitive to the same path lengths. As a consequence, modifying the PLD in the spiral arm model doesn't change the average grammage needed to explain the sub-Fe/Fe and the B/C by the same factor.

The best fit values are a diffusion spectral slope of $\delta = 0.35$ to $\delta = 0.43$, and a diffusion coefficient normalization between $D_0 = 1 \times 10^{27} \mathrm{cm}^2 \mathrm{s}^{-1}$ and $D_0 = 1.5 \times 10^{27} \mathrm{cm}^2 \mathrm{s}^{-1}$ (though the diffusion coefficient range would scale with the halo size, which was chosen here to be 250 pc). To summarize, the consistency found here is one of several successful predictions borne from the spiral arm model:

1. The increase in the positron fraction above ~ 10 GeV is a necessary outcome given that the primary electrons which arrive from a finite distance cool through inverse-Compton and synchrotron radiation while secondary positrons can form locally (Shaviv et al. 2009; Gaggero et al. 2013).

2. The increase in the B/C ratio for $E/\mathrm{nucleon} \lesssim 1$ GeV/nuc. is recovered since the CR age saturates over low energies at the time since the last spiral arm passage (B14).

3. The concentration of CR sources around the galactic spiral arms and lower diffusion coefficient give rise to a temporal variation in the CR flux, seen as 145 Myr cycles in the CR exposure ages behavior of iron meteorites (Shaviv 2003).

4. The smaller halo of the spiral arm model explains the 32 Myr oscillation seen in the 550 Myr long paleoclimatic record (Shaviv et al. 2014).

5. The lower diffusion coefficient implies that the expected anisotropy in the arrival direction of cosmic rays should be smaller by an order of magnitude from predictions of disk-like models with a larger diffusion coefficient, and consistent with the measurements between 1 to 100 TeV (Shaviv et al. 2016).

6. The arm dynamics are responsible for a CR "wake" behind the arms with softer CRs, which give rise to a softer π^0 produced spectrum. Together with the smaller halo, the predicted spectral slope map in γ-rays at around 1-10 GeV is consistent with the FERMI observations (Nava et al. 2016).

7. Last, as we have shown here, the inconsistency between the required diffusion coefficient to fit the B/C and the sub-Fe/Fe ratios is resolved given the different Path Length Distribution.

Thus, the present results introduces further circumstantial evidence to a list that strongly implies that CRs source inhomogeneity plays an important role in CR physics.

REFERENCES

Accardo, L., Aguilar, M., Aisa, D., Alvino, A., Ambrosi, G., Andeen, K., Arruda, L., Attig, N., Azzarello, P., Bachlechner, A., & et al. 2014. High Statistics Measurement of the Positron Fraction in Primary Cosmic Rays of 0.5-500 GeV with the Alpha Magnetic Spectrometer on the International Space Station. Physical Review Letters, **113**(12), 121101.

Adriani, O. et al. 2009. An anomalous positron abundance in cosmic rays with energies 1.5-100GeV. Nature, **458**, 607–609.

Aharonian, F. A., Atoyan, A. M., & Voelk, H. J. 1995. High energy electrons and positrons in cosmic rays as an indicator of the existence of a nearby cosmic tevatron. A&A, **294**, L41–L44.

Ahlers, M., Mertsch, P., & Sarkar, S. 2009. Cosmic ray acceleration in supernova remnants and the FERMI/PAMELA data. Phys. Rev. D, **80**(12), 123017.

Benyamin, D., Nakar, E., Piran, T., & Shaviv, N. J. 2014. Recovering the Observed B/C Ratio in a Dynamic Spiral-armed Cosmic Ray Model. ApJ, **782**, 34.

Bergström, L., Bringmann, T., & Edsjö, J. 2008. New positron spectral features from supersymmetric dark matter: A way to explain the PAMELA data? Phys. Rev. D, **78**(10), 103520.

Binns, W. R., Garrard, T. L., Israel, M. H., Jones, M. D., Kamionkowski, M. P., Klarmann, J., Stone, E. C., & Waddington, C. J. 1988. Cosmic-ray energy spectra between 10 and several hundred GeV per atomic mass unit for elements from Ar-18 to Ni-28 - Results from HEAO 3. ApJ, **324**, 1106–1117.

Blasi, P. 2009. Origin of the Positron Excess in Cosmic Rays. Physical Review Letters, **103**(5), 051104.

Blasi, P., & Serpico, P. D. 2009. High-Energy Antiprotons from Old Supernova Remnants. Physical Review Letters, **103**(8), 081103.

Cesarsky, C. J. 1980. Cosmic-ray confinement in the galaxy. ARA&A, **18**, 289–319.

Chi, X., Cheng, K. S., & Young, E. C. M. 1996. Pulsar Wind Origin of Cosmic Ray Positrons. ApJ, **459**, L83.

Davis, A. J., Mewaldt, R. A., Binns, W. R., Christian, E. R., Cummings, A. C., George, J. S., Hink, P. L., Leske, R. A., von Rosenvinge, T. T., Wiedenbeck, M. E., & Yanasak, N. E. 2000. On the low energy decrease in galactic cosmic ray secondary/primary ratios. Pages 421–424 of: Mewaldt, R. A., Jokipii, J. R., Lee, M. A., Möbius, E., & Zurbuchen, T. H. (eds), Acceleration and Transport of Energetic Particles Observed in the Heliosphere. American Institute of Physics Conference Series, vol. 528.

di Bernardo, G., Evoli, C., Gaggero, D., Grasso, D., & Maccione, L. 2010. Unified interpretation of cosmic ray nuclei and antiproton recent measurements. Astroparticle Physics, **34**, 274–283.

Effenberger, F., Fichtner, H., Scherer, K., & Büsching, I. 2012. Anisotropic diffusion of Galactic cosmic ray protons and their steady-state azimuthal distribution. A&A, **547**, A120.

Gaggero, D., Maccione, L., Di Bernardo, G., Evoli, C., & Grasso, D. 2013. Three-Dimensional Model of Cosmic-Ray Lepton Propagation Reproduces Data from the Alpha Magnetic Spectrometer on the International Space Station. Physical Review Letters, **111**(2), 021102.

Garcia-Munoz, M., Simpson, J. A., Guzik, T. G., Wefel, J. P., & Margolis, S. H. 1987. Cosmic-ray propagation in the Galaxy and in the heliosphere - The path-length distribution at low energy. ApJS, **64**, 269–304.

Harding, A. K., & Ramaty, R. 1987. The Pulsar Contribution to Galactic Cosmic Ray Positrons. Page 92 of: International Cosmic Ray Conference. International Cosmic Ray Conference, vol. 2.

Hareyama, M. 1999. Sub-Fe/Fe ratio obtained by Sanriku balloon experiment. International Cosmic Ray Conference, **3**, 105.

Hooper, D., Blasi, P., & Dario Serpico, P. 2009. Pulsars as the sources of high energy cosmic ray positrons. J. Cos. Astropart. Phys., **1**, 25.

Ibarra, A., & Tran, D. 2008. Antimatter signatures of gravitino dark matter decay. J. Cos. Astropart. Phys., **7**, 2.

Karol, P. J. 1975. Nucleus-nucleus reaction cross sections at high energies: Soft spheres model. Phys. Rev. C, **11**, 1203–1209.

Mannheim, K., & Schlickeiser, R. 1994. Interactions of cosmic ray nuclei. A&A, **286**(June).

Mertsch, P., & Sarkar, S. 2009. Testing Astrophysical Models for the PAMELA Positron Excess with Cosmic Ray Nuclei. Physical Review Letters, **103**(8), 081104.

Moskalenko, I. 2011. Isotopic Production Cross Sections for CR Applications (ISOPROCS Project). International Cosmic Ray Conference, **6**, 283.

Moskalenko, I. V., & Mashnik, S. G. 2003. Evaluation of Production Cross Sections of Li, Be, B in CR. International Cosmic Ray Conference, **4**, 1969.

Moskalenko, I. V., & Strong, A. W. 1998. Production and Propagation of Cosmic-Ray Positrons and Electrons. ApJ, **493**, 694–707.

Nava, L., Benyamin, D., Piran, T., & Shaviv, N. J. 2016. Spectral map of the diffuse γ-ray emission from π^0-decay in a dynamic spiral arm model: comparison with observations. in preparation.

Oliva, A, Collaboration, AMS, et al. . 2013. Precision measurement of the cosmic ray boron-to-carbon ration with AMS. Proceedings 33rd ICRC, Rio de Janeiro.

Profumo, S. 2008. Dissecting cosmic-ray electron-positron data with Occam's Razor: the role of known Pulsars. ArXiv e-prints.

Schwaller, P., Pepin, M., Favier, B., Richard-Serre, C., Measday, D. F., & Renberg, P. U. 1979. Proton total cross sections on ^{1}H, ^{2}H, ^{4}He, ^{9}Be, C and O in the energy range 180 to 560 MeV. Nuclear Physics A, **316**, 317–344.

Shaviv, N. J. 2003. The spiral structure of the Milky Way, cosmic rays, and ice age epochs on Earth. New Astron., **8**, 39–77.

Shaviv, N. J., Nakar, E., & Piran, T. 2009. Inhomogeneity in Cosmic Ray Sources as the Origin of the Electron Spectrum and the PAMELA Anomaly. Physical Review Letters, **103**(11), 111302.

Shaviv, N. J., Benyamin, D., Murase, K., & Piran, T. 2016. Implications of Smaller Cosmic Ray Halo and Diffusion Coefficient to understanding the Knees and Observed Anisotropy. submitted to PRL.

Shaviv, Nir J, Prokoph, Andreas, & Veizer, Ján. 2014. Is the solar system's galactic motion imprinted in the phanerozoic climate? Scientific reports, **4**.

Silberberg, R., & Tsao, C. H. 1990. Spallation processes and nuclear interaction products of cosmic rays. Phys. Rep., **191**, 351–408.

Sisterson, J. M., & Vincent, J. 2006. Cross section measurements for proton-induced reactions in Fe and Ni producing relatively short-lived radionuclides at E$_p$ = 140 500 MeV. Nuclear Instruments and Methods in Physics Research B, **251**, 1–8.

Strong, A. W., & Moskalenko, I. V. 1998. Propagation of Cosmic-Ray Nucleons in the Galaxy. ApJ, **509**, 212–228.

Strong, A. W., Moskalenko, I. V., & Ptuskin, V. S. 2007. Cosmic-Ray Propagation and Interactions in the Galaxy. Annual Review of Nuclear and Particle Science, **57**, 285–327.

Titarenko, Y. E., Batyaev, V. F., Titarenko, A. Y., Butko, M. A., Pavlov, K. V., Florya, S. N., Tikhonov, R. S., Mashnik, S. G., Ignatyuk, A. V., Titarenko, N. N., Gudowski, W., Těšínský, M., Persson, C.-M. L., Abderrahim, H. A., Kumawat, H., & Duarte, H. 2008. Cross sections for nuclide production in a Fe56 target irradiated by 300, 500, 750, 1000, 1500, and 2600 MeV protons compared with data on a hydrogen target irradiated by 300, 500, 750, 1000, and 1500 MeV/nucleon Fe56 ions. Phys. Rev. C, **78**(3), 034615.

Webber, W. R., Soutoul, A., Kish, J. C., & Rockstroh, J. M. 2003. Updated Formula for Calculating Partial Cross Sections for Nuclear Reactions of Nuclei with $Z <= 28$ and $E > 150$ MeV Nucleon^{-1} in Hydrogen Targets. ApJS, **144**, 153–167.

Werner, M., Kissmann, R., Strong, A. W., & Reimer, O. 2013. A new 3D transport and radiation code for galactic cosmic rays. ArXiv e-prints.